Journal of Engineering for Gas Turbines and Power,
139(9), 092501. Paper No: GTP-16-1192

Detailed study on stiffness and load characteristics of film-riding groove types using design of experiments

S.M.Tibos
GE Power
Newbold Road
Rugby
CV21 2NH
United Kingdom
Email: stacie.tibos@ge.com

C.Georgakis
GE Power
Newbold Road
Rugby
CV21 2NH
United Kingdom

K.Harvey
GE Power
Newbold Road
Rugby
CV21 2NH
United Kingdom

J.A.Teixeira
Centre for Power Engineering
Cranfield University
College Road
Cranfield
Bedfordshire MK43 0AL
United Kingdom

In the application of film-riding sealing technology there are various groove features that can be used to induce hydrodynamic lift. However, there is little guidance in selecting the relative parameter settings in order to maximise hydrodynamic load and fluid stiffness. In this study two groove types are investigated; Rayleigh step and inclined groove. The study uses a design of experiments approach and a Reynolds equation solver to explore the design space. Key parameters have been identified that can be used to optimise a seal design. The results indicate that the relationship between parameters is not a simple linear relationship. It was also found that higher pressure drops hinder the hydrodynamic load and stiffness of the seal suggesting an advantage for using hydrostatic load support in such conditions.

Nomenclature

$\dot{m}$	Mass flow (kg/s)
μ	Viscosity (kg/ms)
ρ	Density (kg/m^3)
$\widehat{K}$	Dimensionless stiffness (-)
$\widehat{W}$	Dimensionless load (-)
h	Film height (m)
p	Pressure (Pa)
p_1	Downstream Pressure (Pa)
p_2	Upstream Pressure (Pa)

U	Tangential surface speed (m/s)
A	Seal pad area (m^2)
F	Cell residual value
i	Grid point in axial direction (-)
j	Grid point in circumferential direction (-)
R	Gas constant (J/kgK)
T	Temperature (K)
W	Seal nett load (N)
x	Axial coordinate (m)
y	Circumferential coordinate (m)

1 Introduction

There is a strong demand in power generation turbomachinery for highly efficient, dynamic seals. Advanced sealing technologies are vital in order to achieve higher turbine efficiencies whilst ensuring flexible operation and long lifetime. Future and current trends in the use of renewable energy sources of electricity requires conventional fossil fuel plants to operate more flexibly [1]. This means either accepting larger build clearances or rub events with current sealing technology e.g. labyrinth seals or moving towards non-contacting, rotor-following sealing technologies.

Early attempts to develop a film-riding seal focused mainly on face seals. Designs include the face seal [2], the Double Divert Spiral Groove Face Seal [3], the Aspirating seal [4] and the foil face seal [5]. One of the main challenges reported in literature was the high levels of thermal distortion experienced at the high diameter applications and small film heights [6]. It was considered by Menendez and Cunningham [7] that turbine applications are reaching speed and pressure levels beyond the current capability of face seal technology.

There are various advantages and disadvantages for radial or axial orientation when designing a film-riding seal. This work focuses on the development of a radial mounted film-riding seal (axial flow direction). Application of a seal within a turbomachinery environment often means dealing with a large amount of axial movement, the amount of radial movement is often far less, this favours a radial seal design. Other advantages include being able to track circumferential out of roundness and having easy scalability i.e. by changing the number of segments. A schematic of a radially compliant seal on a steam turbine blade tip can be seen in Figure 1. In recent years there has been a particular focus on non-contacting technology for large diameter turbomachinery application with more emphasis on radial orientated seals.

One example is the Hydrostatic Advanced Low Leakage (HALO) seal [8]. This seal has evolved from the shoed or hybrid brush seal [9]. The HALO seal has additional features on the underside of the pad which enhance the aerodynamic rotor following capability of the seal. The HALO seal generally has two or three grooves/cavities leading to a flat, divergent or convergent-divergent section. The seal has a leading (upstream) edge lip that draws a pad closer to the rotor surface when the seal experiences a pressure differential. The flow becomes choked as the pad approaches the rotor surface and the choked flow produces a force away from the rotor. The dual beam design allows the seal to adjust to these opposing forces as the pressure differential increases and the seal finds its equilibrium balance clearance.

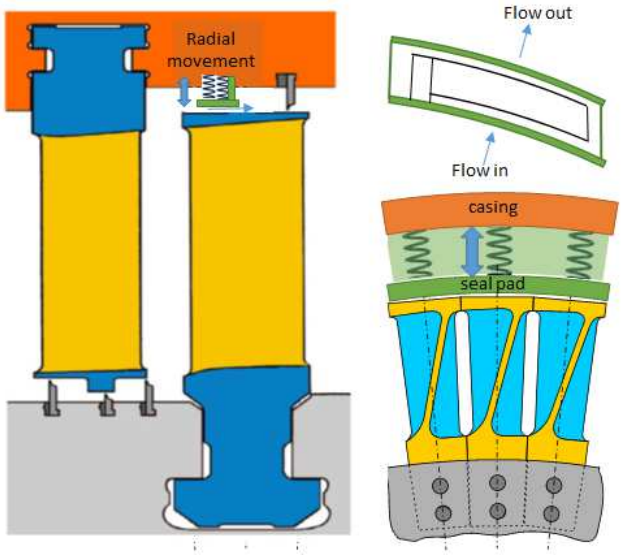

Fig. 1. Schematic of a radially complaint film riding seal on a steam turbine blade tip

Another example is the Film-riding Pressure Activated Leaf Seal (FRPALS) [10, 11]. The FRPALS technology is extended from the PALS technology [12] to include a film-riding pad. This technology works by having a relatively large install gap, one which avoids any contact during start-up, shutdown and transients. The seal has two pivoted layers of frusto-conical plates with overlapped periodic slots. The slots allow for the seal to deflect downwards with low stress under pressure loads. The front facing leaves are designed to deflect under pressure load and the rear layer support the seal pad. The leaves are fixed to the seal pad via curved ankles, which allows for the moments from the leaves to be transmitted to the seal pad whilst helping main parallelism with the shaft.

There are various groove patterns or features that can be used to induce hydrodynamic lift between two sealing faces. DiRusso [13] performed tests to measure the film thickness (face separation) and seal frictional torque as a function of shaft speed for four face seal groove configurations. The geometries tested were a Rayleigh step lift pad, an outward-pumping spiral groove and two inward-pumping spiral groove seal configurations. Some of the geometric parameters were varied including; spiral groove angle, groove to land width ratio, groove depth and the number of grooves. The seal that showed the greatest film thickness and therefore highest stiffness was the inward-pumping, shallow spiral groove design. This groove design was then optimised and the film thickness was then up to 40% higher than any of the other designs. Interestingly, the Rayleigh step lift pad seal had 36% less frictional torque at a speed of 14,000rpm compared to the three spiral groove designs. Tournerie [14] also analysed various groove geometries for face seals. It was found that the optimum spiral groove angle was approx-

imately 17°. Rayleigh steps were also assessed by Cheng [15]. The authors showed that there is very little difference between the spiral groove and Rayleigh pad geometries with the spiral groove showing a slight benefit at off design conditions. The authors used groove parameters that had been optimised for a spiral-groove thrust plate to assess the behaviour of inclined grooves and herringbone grooves. It was shown that inclined grooves located on the high-pressure side gave a larger hydrodynamic lift even when compared to the herringbone groove geometry. However, the herringbone gave the best result when the objective function was both leakage and film stiffness.

Despite the vast amount of research in the design of groove features (particularly face seals) there is no guidance for which geometric parameters are the most important to tune in order to maximise the load and/or stiffness of the fluid. Previous work from the authors [16] have shown that the most promising groove types likely to offer significant fluid load support at as higher film thickness as possible whilst also maintaining the maximum amount of film stiffness are the Rayleigh step, inclined grooves and herringbone grooves. The focus of this work is a detailed assessment that investigates the fluid load and stiffness characteristics of two of these three geometries. This is achieved using a design of experiments approach. Such techniques are becoming increasingly popular in recent years and have already been applied to several sealing problems including brush seals [17] and balance drum seals [18, 19].

The ultimate aim with this study is to determine the key influencing parameters and guide the seal designer towards the optimal groove design.

2 Methodology

In order to predict the hydrodynamic lift of the seal the fluid region must be modelled. This is most commonly achieved by using the Reynolds equation [20–22]. Equation 1 shows the Cartesian formulation of the Reynolds equation.

$$\frac{\partial}{\partial x}(\rho h^3 \frac{\partial p}{\partial x}) + \frac{\partial}{\partial y}(\rho h^3 \frac{\partial p}{\partial y}) = 6\mu U \frac{\partial}{\partial x}(\rho h) \tag{1}$$

As the film height is small compared to the intended radius of application the computational domain is modelled as a flat surface and the curvature is neglected, this approach is frequently applied when studying thin film flow in a radially orientated seal e.g. Finger Seals [22] [23].

To solve the Reynolds equation numerical techniques are often used. This involves some form of discretization, in this case a finite difference formulation. With this method a large sparse system of linear equations is solved directly. The linearisation from the nonlinear form of the Reynolds equation is achieved using the Newton method, as recommended by Szeri [24] and also outlined by Lebeck [20]. The method works by first considering a mass flow balance across a control volume. The control volume and mass flow balance used can be seen in Figure 2.

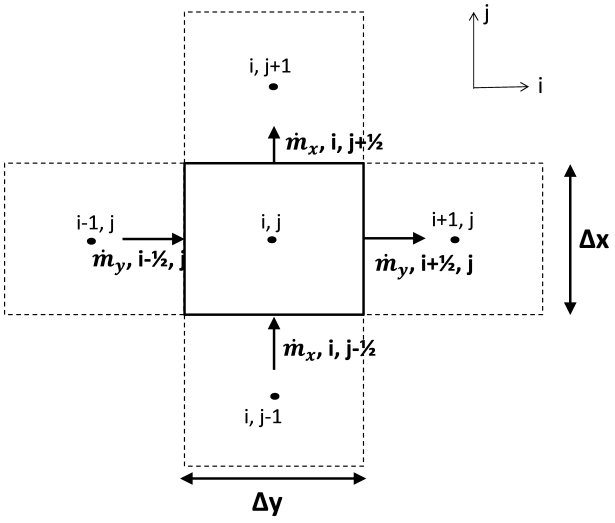

Fig. 2. Finite Difference Control Volume in Cartesian coordinates

Mass flow expressions for each of the four boundaries are derived. For example the mass flow inlet from the left hand vertical wall of the cell is shown here in Equation 2.

$$\dot{m}_{y_{i-\frac{1}{2},j}} = \frac{p_{i-1,j} + p_{i,j}}{2RT}\left[-\frac{h^3_{i-\frac{1}{2},j}}{12\mu}\frac{p_{i,j} - p_{i-1,j}}{\Delta y} + \frac{U h_{i\frac{1}{2},j}}{2}\right]\Delta x \tag{2}$$

An equation for each of the mass flow terms are derived and summed to give the time rate of change of the mass in the control volume, as shown in Equation 3.

$$\dot{m}_{xi-\frac{1}{2},j} - \dot{m}_{xi+\frac{1}{2},j} + \dot{m}_{yi,j-\frac{1}{2}} - \dot{m}_{yi,j+\frac{1}{2}} = F[p] \tag{3}$$

To solve the equation the solution to $F[p] = 0$ at all grid points needs to be found. The Newton method is used to linearise the system of equations; it does this by calculating a set of corrections terms Δp to the preceding estimates. A system of linear equations can be created that can be solved for the pressure correction terms Δp. To find a new estimate of pressure Equation 4 can be used.

$$\left[p^{n+1}\right] = [p^n] + [\Delta p] \tag{4}$$

The pressure correction terms that are then used in Equation 5.

$$F'[p^n][\Delta p] = -F[p^n] \tag{5}$$

In order to solve Equation 5 the matrix of F needs to be created. This matrix must be recreated at each iteration due to the derivatives changing with pressure each time. Therefore solving the equation $F'[p^n][\Delta p] = -F[p^n]$ and updating the estimate $\left[p^{n+1}\right]$ is repeated until the condition of the

equation $F[p] = 0$ is approximated to the accuracy needed. In matrix form the linear system of equations is as shown in Equation 6.

$$\begin{bmatrix} \ddots & \ddots & 0 \\ \ddots & \frac{\delta F_{i,j}}{\delta p_{i,j}} & \ddots \\ 0 & \ddots & \ddots \end{bmatrix} \begin{bmatrix} \vdots \\ \Delta p_{i,j} \\ \vdots \end{bmatrix} = \begin{bmatrix} \vdots \\ -F_{i,j} \\ \vdots \end{bmatrix} \tag{6}$$

The force acting on the underside of the pad can then be found by integrating the pressure over the pad area. This force is the main numerical output from the method.

The method uses a uniform grid, however the groove features are not aligned to the grid. This can create numerical errors in the solution. However, the mesh can be made sufficiently fine so that these errors are minimised. Using a uniform grid as opposed to a conformal grid means a faster solution and one which can be applied to a range of geometries.

A mesh sensitivity study was performed to check mesh density against the accuracy of the solution. The herringbone groove geometry from Proctor and Delgado [25] was chosen as the benchmark for this study. The boundary conditions from their rotational tests were also taken (tangential speed of 54m/s, inlet gauge pressure of 241kPa). The grid density was varied from 10 cells by 10 cells up to 70 cells by 70 cells. The time elapsed per calculation was recorded as well as the dimensionless lift force generated by the geometry. The formula for dimensionless load can be seen in Equation 7. It should be noted that all load and stiffness results presented are dimensionless and therefore factor out the effects from differences in axial or circumferential lengths.

$$\widehat{W} = \frac{W}{(p_2 - p_1)A} \tag{7}$$

Figure 3 shows the trade-off plot for accuracy against computational time. The most suitable grid density was chosen to be a grid of 50 cells by 50 cells. With this grid setting the percentage difference in force compared with the maximum 70 by 70 grid was less than 2% and the computational time was less than 20% of the time for the 70 by 70 grid. The mesh generated for an inclined groove geometry using a 50*by*50 grid can be seen in Figure 4.

The method is formulated with periodic boundaries at the circumferential ends where each groove pattern repeats itself. This periodicity assumes a continuous groove pattern around the circumference with no circumferential pad interstices modelled. However, in reality there would be circumferential gaps between sealing pads and the flow through these gaps would likely have an interaction with the seal gap flow. The modelled section and repeating groove pattern can be seen in Figure 5.

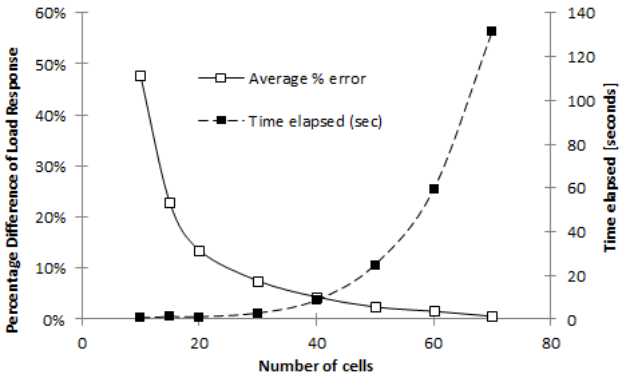

Fig. 3. Trade-off plot for solution accuracy against computational time

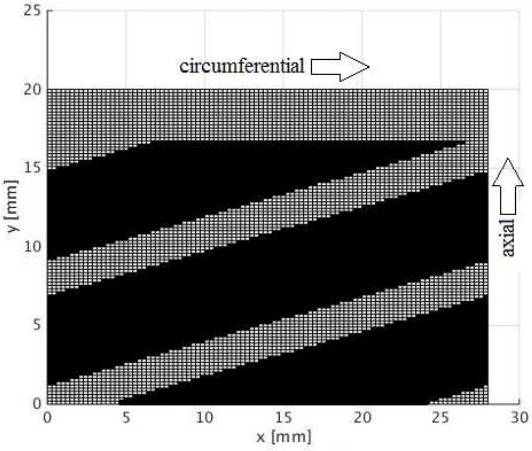

Fig. 4. A discretised geometry for an inclined groove using $50x50$ grid

Fig. 5. Modelled section and repeating groove pattern

3 Rayleigh Step

3.1 Initial Screening

Initial screening is useful when there is very little knowledge available about the system and it is necessary to check as many of the influencing parameters as possible. In a screening design only a fraction of the full factorial design is analysed. Otherwise, with many variables, or many levels of each variable, full factorial simulation can get very large and impractical. By fractioning a design and accept the risk of confounding there can be a significant reduction in the number of configurations to assess.

In order to screen variables for the Rayleigh Step design we need to first include as many of the possible parameters

Table 1. Parameters included in the screening design

Variable	Low level	High level
Land upstream (mm)	1	5
Land downstream (mm)	1	5
Circumferential land (mm)	2	10
Circumferential groove (mm)	10	50
Groove depth (μm)	15	50
Feed groove width (mm)	1	5
Feed groove depth (mm)	5	30
Pad length (mm)	20	40

affecting the performance as we can. Table 1 highlights all the parameters in the screening design including the high and low levels for each variable and Figure 6 shows the parameters that make up the Rayleigh step geometry.

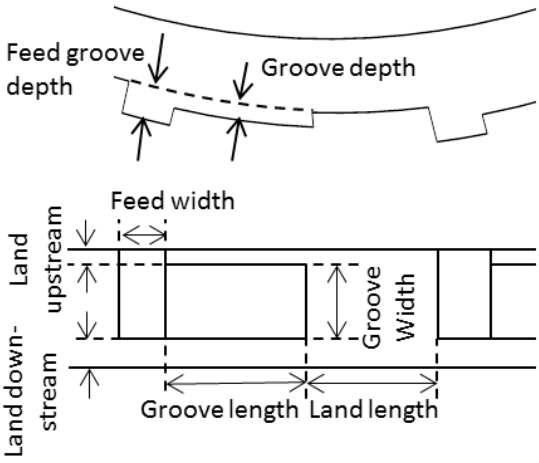

Fig. 6. Rayleigh step geometry

Practical upper and lower limits for each of the parameters have been chosen so that their various combinations all produce practical designs. In reality these limits could be extended however the parameter combinations could produce designs which are nonsensical. In this initial screening design a single operating point is considered. The fluid properties, with air as the working fluid, can be seen in Table 2.

The simulation experimental design has 8 variables at 2 levels each which if done as a full factorial would create 256 cases. A resolution V (level 5 fidelity) simulation experiment was planned using the Minitab software [26] Using a resolution V fractional factorial design means only 64 cases are necessary. Using this experimental design it is possible to see all the two way interactions and identify the 3 way interactions although they are intentionally confounded with

Table 2. Operating conditions used for screening design

Parameter	Units	Value
Pressure upstream	bar	1.15
Pressure downstream	bar	1.0
Temperature	K	300
Viscosity	Pa s	2.0e−5
Film height	μm	17.5
Surface speed	m/s	100
Compressibility	-	Yes

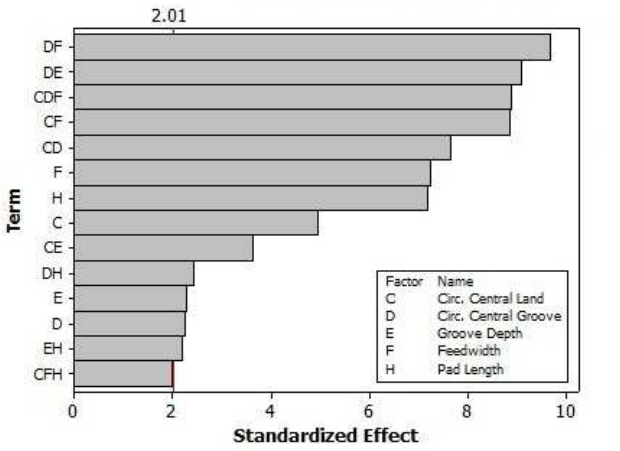

Fig. 7. Pareto chart for the reduced model

other 2 way interactions. For the purpose of initial screening this resolution is deemed sufficient. Other screening designs, such as Plackett-Burman could be used. However, the resolution would be too low as two way interactions would be confounded with main effects.

The Pareto plot for a reduced version of the model can be seen in Figure 7 (only the top 14 variables and any hierarchical parameters are included) and Figure 8 shows the main effects plot for the Rayleigh step design.

Figure 8 demonstrates that the feed groove width, pad length and circumferential land are having the largest single effect on the response. Interestingly, the reduced model Pareto plot shows that the largest effects are two way interactions. More specifically, the interaction of circumferential groove width with both the feed groove width and the groove depth. A significant 3 way interaction also exists between the circumferential land, circumferential groove width and the feed groove width. The interactions were assessed using an interaction plot which showed that the less influential parameters; upstream land, downstream land and feed groove depth also have little or no interaction with other parameters.

By consulting the Pareto plot, main effects plot and interaction plot it is prudent to fix upstream land, downstream land and feed groove depth in the further refined model. By

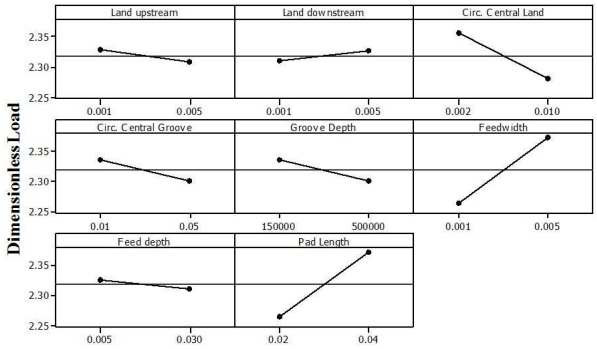

Fig. 8. Main effects plot for Rayleigh step screening parameters

Table 3. Parameters included in the quarter factorial design

Variable	Low level	High level
Circumferential land (mm)	1.5	3
Circumferential groove (mm)	10	50
Groove depth (μm)	15	40
Feed width (mm)	3	7
Downstream pressure (bar)	1	10
Pressure drop (bar)	1	5
Film Height (μm)	10	25
Surface speed (m/s)	50	150

inspecting the main effects plot it is clear that there is some marginal advantage to setting the upstream land and feed groove depth to their low values and the downstream land to its high value. The pad length is often a geometric constraint, the higher value setting was chosen as it generates the strongest response and therefore any trends in the data are attenuated. The results are also useful in re-adjusting the upper and lower limits of the design space to more pertinent levels.

3.2 Quarter Factorial Analysis

The purpose of the initial screening was to understand how the geometric parameters (control factors) influence the design. The operational variables that are known to have a large effect on performance were not varied. For the following quarter factorial analysis these boundary conditions are included in the simulation experimental design. Namely film height, surface speed, downstream pressure and pressure drop. The four operating parameters and the four remaining geometric parameters can therefore be combined in a second simulation experimental design. In this second design the geometric design space is narrowed and a centre point is added to give an indication of curvature and linear fit of the model. To limit the number of cases the design is set to resolution V which makes this set of analyses a quarter factorial design. The parameter list, including high and low levels, for the quarter factorial design can be seen in Table 3.

It should also be noted that the large range for speed (50-150 rpm) relates to the machine requirements whereby the seal will be applied to both low and high radius applications in power generation turbomachinery.

As the interest is not only in the load generated by the seal but also the stiffness this can be included as a second response. The formula for dimensionless stiffness can be seen in Equation 8.

$$\widehat{K} = \frac{dF}{dh}\frac{h}{(p_2 - p_1)A} \tag{8}$$

The refined Pareto plots for both dimensionless load and dimensionless stiffness can be seen in Figure 9 and Figure 10 respectively.

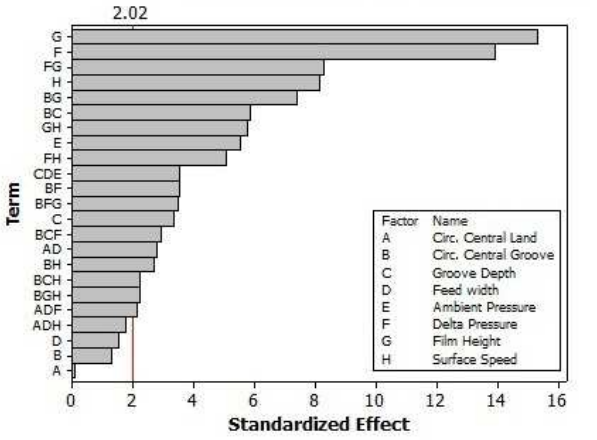

Fig. 9. Reduced model Pareto chart dimensionless load

It is clear that the largest effects on both load and stiffness are the pressure drop, surface speed and film height. The interaction of film height with circumferential groove length and pressure drop is also significant for both load and stiffness. The effect of downstream (ambient) pressure is only significant for load but not stiffness. Most interesting of all is the strong effect of circumferential groove length on stiffness which is far weaker for load. This parameter could potentially be used to tune the design to improve stiffness without having any detrimental effect on load.

The analysis using the reduced model also shows that the relationship between parameters has significant second order curvature effects. This is demonstrated by the observed values for curvature in the model of 0.0060 and 0.0017 for dimensionless load and dimensionless stiffness respectively. As these values are below the level for statistical significance ($p < 0.05$) this second order curvature effect is confirmed. However, the fit of the models is reasonably good with adjusted R-squared values of 80.7% and 92.7% for dimensionless load and dimensionless stiffness respectively.

As well as the strength of the parameters effects on the

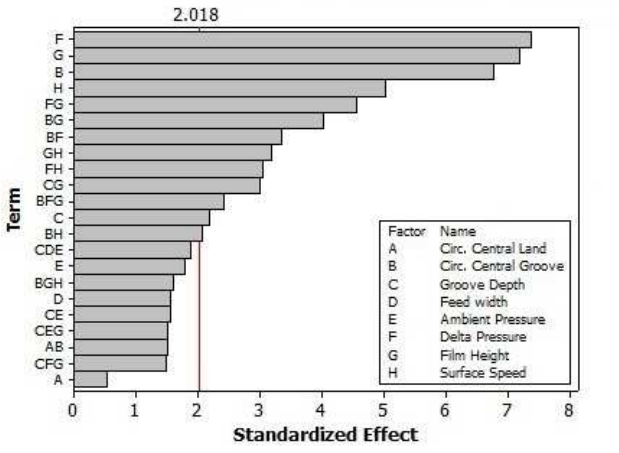

Fig. 10. Reduced model Pareto chart dimensionless stiffness

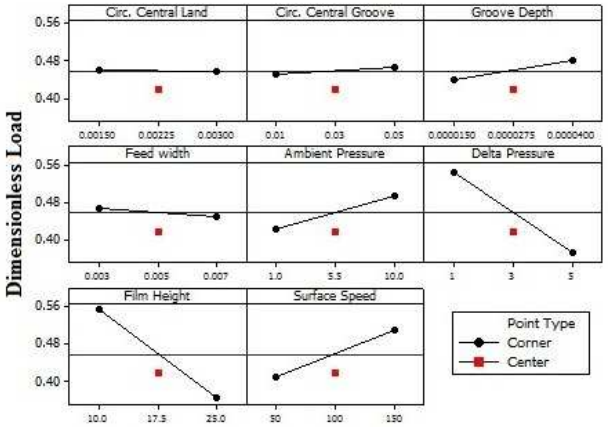

Fig. 11. Main effects plot for dimensionless load

response it is also interesting to look at the direction of those responses. To do this we can examine the main effects plots. These are shown in Figure 11 and Figure 12 for dimensionless load and stiffness respectively.

The main effects plots show that by having a higher pressure drop the hydrodynamic load and stiffness of the seal can be hindered. This is also the case if we have a lower downstream pressure. However, the pressure drop has a significantly higher effect compared to downstream (ambient pressure). The main effects plot also show that both feed groove width and circumferential land have a mild effect on stiffness but a particularly weak effect on load. In order to fix these parameters for future analysis it must be ensured that they are not strongly interacting with any other parameters. This can be done by examining the Pareto plots in Figure 9 and Figure 10. The Pareto plots show that both feed groove width and circumferential land are not found in any of the significant effects on either load or stiffness. However, they do have a significant interaction with each other in terms of load.

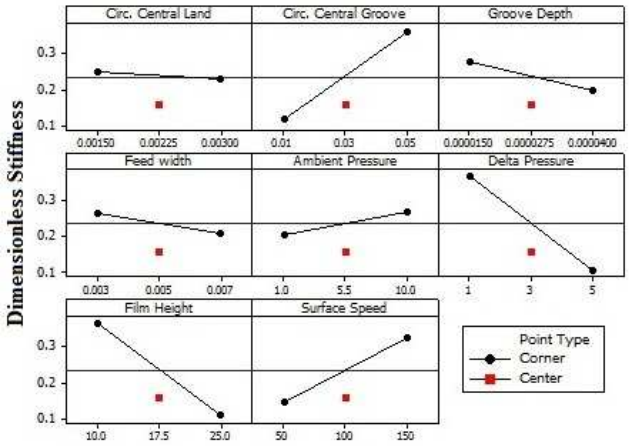

Fig. 12. Main effects plot for dimensionless stiffness

4 Inclined Grooves

To assess the behaviour and performance of the inclined groove a similar process as the one taken for the Rayleigh step groove type is followed. In the analysis for the inclined groove the matrix was now automated using a script. By doing this, many simulations can be run in the background and the requirement for keeping the number of levels to a minimum is less important. In a screening design only a fraction of the full factorial design is usually run. However, for this second groove type a full factorial design is now possible using the automation script. This also removes the risk of confounding the variables.

4.1 Initial Screening

In order to begin to understand the inclined groove all the geometric parameters that could affect the design are listed while also determining sensible high and low values. The parameters used in the initial factorial design can be seen in Table 4. Figure 13 shows the parameters that define the inclined groove design. The operating conditions are the same as those used for the Rayleigh step in Table 2.

The results from the initial full-factorial design show some of the important parameters (modelled terms are reduced down to include only the top 30 variables). This is

Table 4. Parameters included in the initial full-factorial design

Variable	Low level	High level
Land upstream (mm)	0	1
Land downstream (mm)	5	10
Circumferential land (mm)	10	40
Circumferential groove (mm)	10	40
Groove depth (μm)	20	60
Groove angle (deg)	10	30
Pad length (mm)	20	30

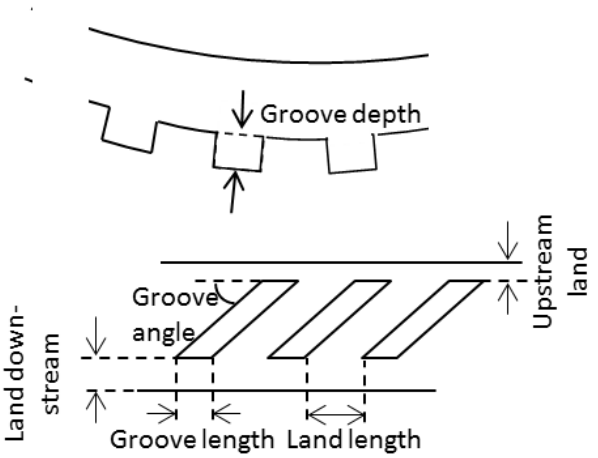

Fig. 13. Inclined groove geometry

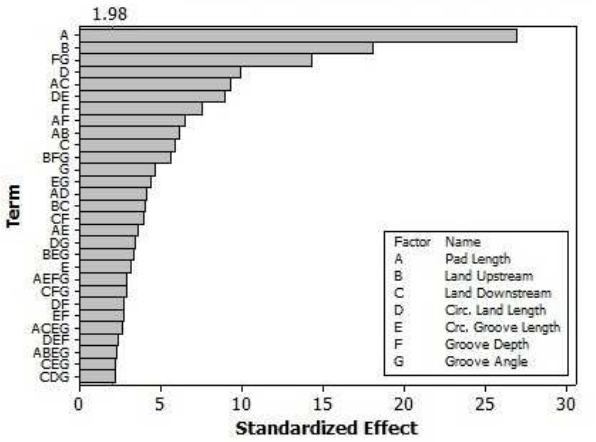

Fig. 14. Pareto chart for inclined groove initial model

shown in Figure 14. It can be seen that the upstream land, pad length and circumferential land all have a significant effect on the load response. Whereas the circumferential groove has the weakest effect on the load. This is further evidenced by the main effects plot in Figure 15. This initial simulation run also shows that there are a number of significant two way interactions with the following noteworthy; pad length with land downstream, groove depth width groove angle, circumferential land with circumferential groove, and pad length with groove depth.

The interaction plot also shows that the most influential parameters; pad length and land upstream have little or no interaction with other parameters. These variables can therefore safely be set at their strongest setting for future analyses. This is also the case for land downstream which is strongest at its highest setting. For the case of the land upstream this means setting the parameter to zero which means the grooves are open to the upstream pressure which is a typically way that inclined grooves can be implemented. The results are also useful in re-adjusting the upper and lower limits of the design space to more appropriate levels.

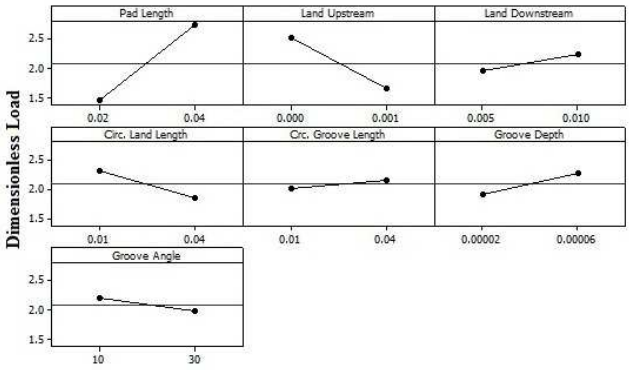

Fig. 15. Main effects plot for inclined groove initial factorial design

Table 5. Parameters included in the second full-factorial design

Variable	Low level	High level
Circumferential land (mm)	10	30
Circumferential groove (mm)	15	50
Groove depth (μm)	30	60
Groove angle (deg)	10	30
Downstream pressure (bar)	1	10
Pressure drop (bar)	1	5
Film Height (μm)	15	25
Surface speed (m/s)	50	150

4.2 Full-Factorial Analysis

The purpose of the initial full-factorial was to understand how the geometric parameters influence the design. As with the Rayleigh step screening analysis, any variables that are known to have a large effect on performance were not varied i.e. film height, surface speed, downstream pressure and pressure drop. For the second set of simulation runs it is important to aim for a more complete understanding of the design space and how the seal will behave under various operating conditions. Therefore these parameters are now included. The four operating parameters and the four remaining geometric parameters can therefore be combined in a second simulation experimental design. In this second analysis the geometric design space is narrowed and a centre point is added to give an indication of curvature and linear fit of the model. As with the initial factorial design for inclined grooves the computations are automated using a script and therefore reduced simulation runs are not as necessary. The parameter list including high and low levels for the quarter factorial design can be seen in Table 5.

The stiffness is also an important parameter and is thus included as a second output response from the simulations. The reduced model Pareto plots for both dimensionless load and dimensionless stiffness can be seen in Figure 16 and Figure 17 respectively. The analysis using the reduced model

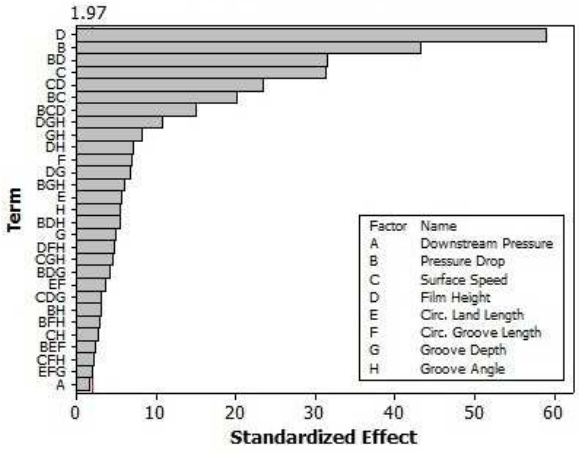

Fig. 16. Reduced model Pareto chart dimensionless load

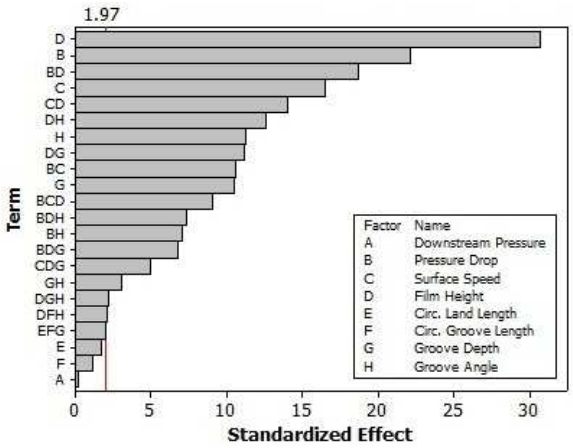

Fig. 17. Reduced model Pareto chart dimensionless stiffness

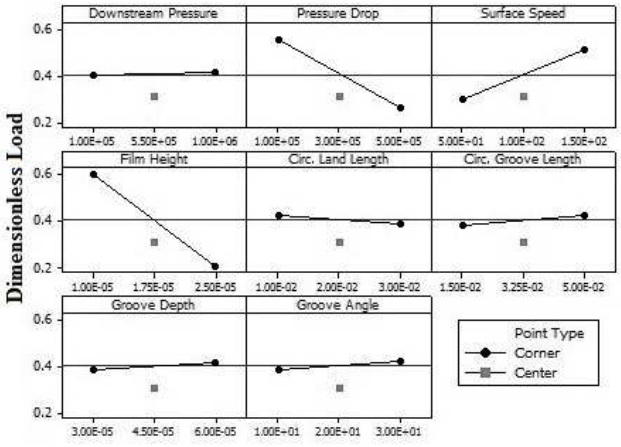

Fig. 18. Main effects plot for dimensionless load

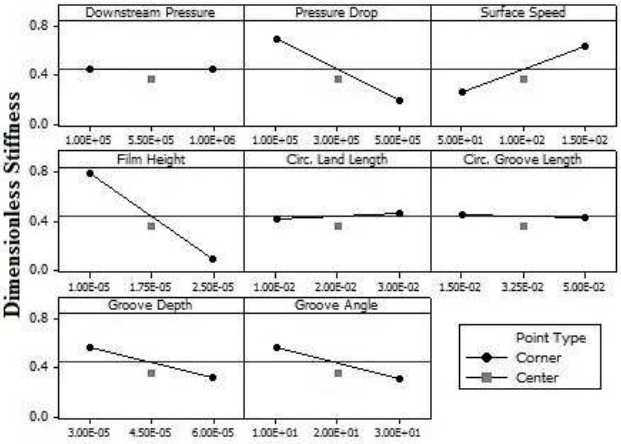

Fig. 19. Main effects plot for dimensionless stiffness

shows that the relationship between parameters has significant second order curvature effects. However, the fit of the models is good with adjusted R-squared values of 97.3% and 92.5% for dimensionless load and stiffness respectively.

It is clear that the largest effects on both load and stiffness are the pressure drop, surface speed and film height. Interestingly the downstream (or ambient) pressure does not have a statistically significant effect on either load or stiffness.

The interaction of pressure drop with film height is significant for both load and stiffness. Most interesting of all is the weak effect of all the geometric parameters particularly on load. The strongest geometric effect comes from the interaction of groove angle and groove depth. The strongest independent geometric effect comes from circumferential groove. However the circumferential groove has a much weaker effect on stiffness. The largest geometric effect on stiffness comes from the groove angle, both independently and interacting with film height. This is also the case for groove depth. At their current settings circumferential groove and circumferential land do not have any significant effect on stiffness. The strength of the geometric and operational parameters for both load and stiffness can be seen in Figure 18 and Figure 19.

5 Discussion

Various factorial (full and partial) designs have been used to investigate and quantify the effects of geometric and operational parameters on the load and stiffness responses of two hydrodynamic groove types. Generally, the geometric parameters have a much weaker effect on both load and stiffness compared to the operational parameters. However, there are many insightful observations that can be made that bring further knowledge and understanding to the seal designer.

There are several parameters that make up a design of a Rayleigh step that can be set to sensible values without having a big impact on the behaviour. Upstream land, downstream land and feed groove depth all have a limited impact on the response while also having little or no interaction with other parameters. The key parameters for changing the design (assuming a limitation on axial pad length) are; the circumferential groove length, groove depth and feed groove

Table 6. Rayleigh Step: Summary of key variables

Variable	LOAD	STIFFNESS
Land upstream	WEAK	WEAK
Land downstream	WEAK	WEAK
Circ. land	MED	WEAK
Circ. groove	MED	STRONG
Groove depth	MED	MED
Feed width	MED	MED
Feed depth	WEAK	WEAK
Pad length	STRONG	MED

Table 7. Inclined Groove: Summary of key variables

Variable	LOAD	STIFFNESS
Land Upstream	N/A(x=0)	N/A
Land Downstream	MED	MED
Circ. land	MED	WEAK
Circ. groove	MED	WEAK
Groove Depth	MED	MED
Groove angle	MED	MED
Pad length	STRONG	STRONG

width. These three parameters control the size of the pocket and the flow area at inlet to the pocket. The flow entering this cavity is forced across the step bearing edge which is the main mechanism for generating hydrodynamic force.

Most interesting of all is the strong effect of circumferential groove length on stiffness which is much weaker for load. This parameter could potentially be used to tune the design to improve stiffness without having any detrimental effect on load. A summary of the key parameters and their level of effect on response can be seen in Table 6.

With regards to the inclined groove type the strongest geometric effect on load comes from the interaction of groove angle and groove depth. These two parameters control the balance between the pumping action created by the inclined groove channels and the hydrodynamic fluid shearing forces generated from the groove edges. The strongest independent geometric effect on load comes from circumferential groove length. However the circumferential groove length has a weaker effect on stiffness as opposed to load which is the opposite trend compared to the Rayleigh step design. This is because when the groove width is large compared to the groove land the design generates less hydrodyanmic force from the angled bearing edges but generates more hydrostatic force from the increased length of the downstream restricting edge. Designs that produce more hydrostatic force generally produce lower fluid stiffness compared to those that generate more hydrodyanmic force. To get the best response from the inclined groove design the groove angle and groove depth should be set at (or near) their high settings. By doing this there is some sacrifice in mean stiffness response, however, the increase in mean load is significant. A summary of the key parameters and their level of effect on response can be seen in Table 7.

For both of the groove designs the modelling shows that the relationship between parameters has significant second order curvature effects. Therefore in order to capture a detailed trend from each individual parameter a number of points should be used to populate the design space. In this study only two levels were chosen for each parameter as this gives an understanding of design trends for the least computational cost. Centre points have been added to the simulation experimental design for an understanding of linearity and the associated computational cost increase was negligible. However, further parameter levels would be required for a more detailed view of the parameter trends.

It is clear that by having a pad that is longer in the axial direction the stiffness and load response can be greatly improved (load and stiffness are non-dimensional and pad area is factored out). Thus the seal designer should seek to use as much axial space as possible for the design of the seal. However, increasing the axial length of the pad, and therefore area, should be done while also considering the increase in heat generated from the viscous shearing of the thin fluid film. To this end, there would likely be a trade-off.

The main effects plots for both groove types also show that by having a higher pressure drop we are actually hindering the hydrodynamic load and stiffness of the seal. This would suggest that at a threshold pressure drop it would be more advantageous to have a seal that utilised mostly hydrostatic lift as opposed to hydrodynamic lift. However, for gas turbine rim location, where pressure differential is low but tangential speed is high the seal must be at least hydrodynamic in nature [27]. Locations in steam turbines such as shaft balance pistons may benefit from a focus on hydrostatically balanced seals as opposed to a hydrodynamic seal. In these locations there is also far more overall force available to move and balance the seal pads.

In both groove design types it is clear that downstream pressure has little effect on the size of the response for either load or stiffness. This means that the operating pressure is not a concern for the reliability in generating hydrodynamic lift for the two groove types assessed up to ambient pressures of 10 bar.

The operating parameters dominate the response of the system and can also interact strongly with some of the geometric parameters. It would therefore be prudent to include all geometric and operational parameters upfront in any future screening studies. Otherwise there is a risk that key parameters may be removed that might later have some significant effect. Similiar guidance is given for including stiffness as an output response as part of the screening.

The authors of this paper chose to use factorial designs in the second sets of simulation experiments for each groove

type in order to understand the main influencing parameters. There are in fact a number of possible experimental designs that could be used e.g. Latin Hypercube or Box-Behnken. Some of these designs may provide a deeper understanding of the design space and also offer more information on the linearity of parameter relationships.

6 Conclusions

Both of the groove types investigated; Rayleigh step and inclined groove have a number of identified geometric parameters that are likely to have only minimal effect on the load and stiffness of the fluid. These parameters can be set at their preferential settings and any higher fidelity design optimisations can focus only on the parameters with strong or medium effects on the responses.

Generally, the geometric parameters have a much weaker effect on both load and stiffness compared to the operational parameters. The designing of the grooves should be tailored carefully to the operational conditions.

For both of the groove designs the modelling shows that the relationship between parameters has significant second order curvature effects. Therefore in order to capture a detailed trend from each individual parameter a number of points should be used to populate the design space.

The results show that a higher pressure drop actually hinders the hydrodynamic load and stiffness of the seal. This may suggest that it is more advantageous to have a seal that utilises hydrostatic load as opposed to hydrodynamic load when large pressure differentials are required. For both groove design types it is clear that downstream pressure has little effect on the size of the response for either load or stiffness.

References

[1] Messenger, A., Williams, R., Ingram, G., Hogg, S., Tibos, S., and Seaton, J., 2015. "A dynamic clearance seal for steam turbine application". ASME Paper No. GT2015-43471.

[2] Munson, J., 1993. "Testing of a high performance compressor discharge seal". Paper No. AIAA 931997.

[3] Berard, G., and Zheng, X., 2008. "Development of Non-Contacting, Low-Leakage, Large-Diameter Air Seal". Paper No. AIAA 2008-4507.

[4] Turnquist, N. A., Tseng, T. W., McNickle, A. D., Athavale, M., and Steinetz, B. M., 1999. "Analysis and full scale testing of an aspirating face seal with improved flow isolation". Paper No. AIAA 1998-3285.

[5] Munson, J., Grant, D., and Agrawal, G., 2002. "Foil Face Seal Proof-of-Concept Demonstration Testing". Paper No. AIAA 2002-3791.

[6] Gardner, J., 1999. "Development of a high speed, high temperature compressor discharge seal". Paper No. AIAA 1999-2684.

[7] Menendez, R., and Cunningham, M., 1999. "Development of liftoff seal technology for air-oil axial sealing applications". Paper No. AIAA 1999-2822.

[8] San Andres, L., and Anderson, A., 2014. "An all-metal compliant seal versus a labyrinth seal: A comparison of gas leakage at high temperatures". ASME Paper No. GT2014-25572.

[9] Justak, J., and Crudgington, P., 2006. "Evaluation of a film riding hybrid seal". Paper No. AIAA 2006-4932.

[10] Grondahl, C. M., and Dudley, J. C., 2010. "Film-riding leaf seals for improved shaft sealing". Paper No. GT2010-23629.

[11] Kirk, T., Bowsher, A., Crudgington, P., Pawlak, A., Grondahl, C. M., and Dudley, J., 2016. "Film riding pressure activated leaf seal proof of concept". Paper No. AIAA 2016-4920.

[12] Grondahl, C. M., 2009. "Pressure activated leaf seal feasibility study and demonstration". Paper No. AIAA 2009-5167.

[13] DiRusso, E., 1982. Film Thickness Measurements for Spiral Groove and Rayleigh Step Lift Pad Self-Acting Face Seals - NASA Technical Paper 2058. Tech. rep.

[14] Tournerie, B., Huitric, J., Bonneau, D., and Frene, J., 1994. "Optimisation and performance prediction of grooved face seals for gases and liquids". In 14th International Conference Fluid Sealing, p. 16.

[15] Cheng, H. S., Chow, C. Y., and Wilcock, D. F., 1968. "Behavior of hydrostatic and hydrodynamic noncontacting face seals.". *J. Lubr. Technol.*(April), pp. 510–519.

[16] Tibos, S., Teixeira, J. A., and Georgakis, C., 2017. "Investigation of the most beneficial groove shape for a film-riding seal". *J. Eng. Gas Turbines Power*.

[17] Pekris, M. J., Franceschini, G., and Gillespie, D. R. H., 2011. "Effect of geometric changes in an idealised contacting brush seal bristle pack on typical key performance measures". ASME Paper No. GT2011-46492.

[18] Untaroiu, A., Liu, C., Migliorini, P. J., Wood, H. G., and Untaroiu, C. D., 2014. "Hole-pattern seals performance evaluation using computational fluid dynamics and design of experiment techniques". *J. Eng. Gas Turbines Power,* **136**(10).

[19] Morgan, N. R., Untaroiu, A., Migliorini, P. J., and Wood, H. G., 2014. "Hole-pattern seals performance evaluation using computational fluid dynamics and design of experiment techniques". *J. Eng. Gas Turbines Power,* **137**(3).

[20] Lebeck, A., 1991. *Principles and Design of Mechanical Face Seals*, illustrate ed. John Wiley & Sons, Inc.

[21] Galimutti, P., Sawicki, J., and Fleming, D., 2009. "Analysis of finger seal lift pads". ASME Paper No. GT2009-59842.

[22] Temis, J. M., Selivanov, A. V., and Dzeva, I. J., 2013. "Finger seal design based on fluid-solid interaction model". ASME Paper No. GT2013-95701.

[23] Yue, G., Zheng, Q., and Zhu, R., 2008. "Numerical simulation of a padded finger seal". ASME Paper No. GT2008-50997.

[24] Szeri, A. Z., 1980. *Tribology, Friction, Lubrication, and Wear*. McGraw-Hill, New York.

[25] Proctor, M., and Delgado, I., 2008. "Preliminary test

results of a non-contacting finger seal on a herringbone-grooved rotor". Paper No. AIAA 2008-4506.
[26] *Minitab 17 Statistical Software (2010). [Computer software]. Minitab, Inc.* State College, PA.
[27] Munson, J., Grant, D., and Agrawal, G., 2001. "Foil face seal development". Paper No. AIAA 2001-3483.

Detailed study on stiffness and load characteristics of film-riding groove types using design of experiments

Tibos, S. M.

2017-04-11

S.M. Tibos, C. Georgakis, K. Harvey and J.A. Teixeira. Detailed study on stiffness and load characteristics of film-riding groove types using design of experiments. Journal of Engineering for Gas Turbines and Power, Vol.139, Iss.9, 092501. Paper No: GTP-16-1192
http://dx.doi.org/10.1115/1.4036058